RSC Advances

PAPER

View Article Online
View Journal | View Issue

Check for updates

Cite this: *RSC Adv.*, 2024, **14**, 10644

# Hydrogenation of cyclohexene over single-atom Pt or Pd incorporated porous ceria nanoparticles under solvent-free conditions

Amal A. Atran and Mohamed S. Hamdy *

In order to maximize the utilization of noble metals in catalysis, single atom of palladium (Pd) and platinum (Pt) were incorporated individually in the framework of porous ceria ($CeO_2$) by using a one-step flash combustion method. Samples with different Pd and Pt loading (0.5, 1, 2.5, and 5 wt%) were prepared and examined by using different analysis techniques such as XRD, ICP, $N_2$ sorption measurements, SEM, HR-TEM, and XPS. The characterization data confirms the formation of zero-state single-atom Pt and Pd (with possible formation of Pd nanoparticles with a size less than 5 nm) incorporated onto the three-dimensional porous ceria structure. The catalytic activity of the synthesized materials was studied in the cyclohexene reduction to cyclohexane at 393 K and 3 atm of pure hydrogen ($H_2$) gas as a model reaction. The obtained results demonstrated that the conversion percentage of cyclohexene is increasing with Pd or Pt loading. The best cyclohexene conversion, 21% and 29%, was achieved over the sample that contains 5 wt% of Pt and Pd, respectively. The collected catalytic data fit the zero-order reaction model, and the rate constant of each catalyst was determined. The catalytic experiments of the most-performed catalysts were repeated five times and the obtained loss in activity was insignificant.

Received 24th February 2024
Accepted 25th March 2024

DOI: 10.1039/d4ra01432d

rsc.li/rsc-advances

Open Access Article. Published on 02 April 2024. Downloaded on 2/12/2026 6:44:27 AM.
This article is licensed under a Creative Commons Attribution-NonCommercial 3.0 Unported Licence.

## 1. Introduction

Hydrogenation reactions are chemical processes that include the conversion of unsaturated double bonds into saturated bonds, resulting in the formation of a new product *via* a reduction mechanism. This type of reaction finds widespread application, particularly in organic substrates containing unsaturated C–C bonds.[1] Hydrogenation became one of the most significant catalytic reactions during the last century, particularly in the fields of agrochemicals, medicines, and large-scale manufacturing of commodities such as ammonia and methanol. Its history dates back to 1823, when finely distributed platinum was utilized in the interaction of oxygen and elemental hydrogen to generate water. Sabatier was the first to perform hydrogenation on hydrocarbons using a Ni catalyst around 70 years later.[2,3] In the early twentieth century, industrial hydrogenation to produce economically significant compounds like methanol and ammonia was primarily based on supported or bulk metals like as Ni, Pd, or Pt. However, the early catalytic transformations were mostly carried out in a heterogeneous way, with the most prominent process being the Haber–Bosch synthesis of $NH_3$. The groundwork for the use of homogeneous systems was created in the 1960 when Wilkinson initially described his famous Rh-based catalyst.[4]

The catalytic heterogeneous hydrogenation of benzene serves as a prime example of a large-scale commercial hydrogenation process, producing cyclohexane in a single step. The hydrogenation of cycloalkenes is regarded as one of the most significant reactions in the industrial field, owing to the generation of highly valuable products.[5] For example, cyclopentane finds its applications in diverse industrial procedures, which encompass resin manufacturing, the rubber industry, and the production of polyurethane foam. Furthermore, the direct reduction of cyclohexene results in the production of cyclohexane, which serves as the principal reactant in the production of Nylon 6 and 6,6.[6] The reduction of cycloalkenes utilizing hydrogen gas is a momentous reaction that possesses substantial industrial ramifications, particularly when executed in the liquid phase at standard temperature and pressure.[7] The hydrogenation of cycloalkenes has been extensively investigated in the liquid phase at ambient temperatures using homogeneous catalysts, including Wilkinson-type catalysts and various transition metal complexes. However, considering environmental and economic considerations, heterogeneous catalysis is of significant value in industrial applications. Therefore, the hydrogenation of cycloalkenes has been thoroughly studied, utilizing supported noble metals and metal oxides.[8] Catalytic hydrogenation, being a bimolecular process, involves the adsorption of hydrogen and unsaturated alkenes to the catalytic surface. Consequently, conducting cycloalkene hydrogenation in a heterogeneous catalytic system introduces various factors, including those associated with catalytic materials such as

*Catalysis Research Group (CRG), Department of Chemistry, College of Science, King Khalid University, P.O Box 9004, Abha 61413, Saudi Arabia. E-mail: m.s.hamdy@gmail.com; mhsaad@kku.edu.sa*



© 2024 The Author(s). Published by the Royal Society of Chemistry

Open Access Article. Published on 02 April 2024. Downloaded on 2/12/2026 6:44:27 AM.
This article is licensed under a Creative Commons Attribution-NonCommercial 3.0 Unported Licence.

metal type and shape, metal loading, and support type. Noble metals have exhibited remarkable activity in heterogeneous hydrogenation processes. As examples, platinum (Pt),[9] rhodium (Rh),[10] ruthenium (Ru),[11] and palladium (Pd)[12] have been widely employed in the hydrogenation of cycloalkenes due to their high activity and stability. However, in light of the challenges associated with the agglomeration of nanopowders and the high cost of noble metals, researchers have adopted a cost-effective strategy. They employ inexpensive means to accommodate limited quantities of precious metals, attaining elevated efficacy through a more economical methodology. In order to mitigate the total expense of the hydrogenation procedure, one approach entails the careful selection of a fitting substrate for the employed nanoparticles of noble metals. An optimal substrate ought to facilitate the heterogeneous catalytic reaction mechanism, diminishing the duration of the chemical process, consequently augmenting output and minimizing the costs associated with production. Various supports, including metal oxides,[13] zeolites,[14] and silica,[15] have been used for this purpose. As an exemplification, Feil *et al.*[16] provided a detailed account of the procedure for depositing palladium nanoparticles onto SBA-15 mesoporous material. The resulting catalyst was subsequently employed for the purpose of catalyzing the reduction of cyclohexene, particularly under conditions of elevated temperatures and pressures, specifically at 75 °C and 4 bar of hydrogen gas. Similarly, Patel *et al.*[17] utilized MCM-41 mesoporous siliceous material to accommodate palladium nanoparticles in combination with monocularly silicotungstate. The fabricated catalyst demonstrated remarkable effectiveness in the hydrogenation of cyclohexene at a temperature of 80 °C and under a hydrogen gas pressure of 10 bar. In an all-encompassing investigation, Hamdy *et al.* explored the hydrogenation of cycloalkenes in a solvent-free liquid-phase utilizing metal nanoparticles supported by mesoporous silica TUD-1 under ambient conditions.[18,19]

The use of $CeO_2$-supported catalysts, particularly those incorporating noble metals, has become a focal point of extensive research. This is attributed to their immense significance in both fundamental academic studies and industrial applications. To take use of $CeO_2$'s oxygen storage and release capabilities, researchers typically incorporate metals into ceria lattice. The incorporation of noble metal species as active sites can markedly enhance catalytic activity due to the distinctive synergy between these noble metal species and $CeO_2$. Despite the substantial improvement in activity, these catalysts encounter challenges such as restricted availability and elevated costs. Consequently, there is a burgeoning research focus on advancing ceria-based catalysts as an alternative approach.

In the last decade, single-atom catalysis has emerged as a rapidly advancing research area, has revitalized the heterogeneous catalysis research horizon. Single-atom catalysts (SACs), distinguished by individual metal sites anchored to solid supports, facilitate optimal metal dispersion and utilization. These isolated, single-atomic active sites demonstrate exceptional catalytic activities in a variety of reactions, efficiently activating fundamental molecules such as $O_2$, $H_2O$, CO, $CO_2$, and $CH_4$.[20,21]

Nowadays, many types of noble metal atoms may be well disseminated onto $CeO_2$ supports using different preparation procedures, such as deposition–precipitation Pt–$CeO_2$ [22] impregnation Pd–$CeO_2$,[23] and Pt–$CeO_2$.[24] Datye *et al.* also devised an "atom-trapping" technique to create thermally stable noble metal $CeO_2$ single atom catalysis. $CeO_2$ can capture and stabilize noble metal single atoms at high temperatures (750–800 °C) because of a strong metal-support interaction. The as-derived catalysts demonstrated much higher sintering stability.[25] Wu *et al.* employed co-precipitation to disperse single atoms of Ru in $CeO_2$, and the resultant catalyst exhibited notable selectivity for azoxybenzene (88.2% selectivity and 17.9% conversion).[26]

In the current study, a one-step combustion method is employed to prepare efficient and distinctive catalysts for hydrogenation reactions. These catalysts consist of a single-atom of a noble metal (Pd and Pt) loaded onto oxygen-vacancies rich porous cerium oxide nanoparticles. The physicochemical properties of the prepared catalysts are studied by XRD, SEM, $N_2$-sorption, HAADF, and HR-TEM. Moreover, the catalytic activity of the synthesized catalysts was assessed in the solvent-free hydrogenation of cyclohexene to cyclohexane as a model reaction. Moreover, a kinetic study was conducted as well as the reusability of the investigated catalysts.

## 2. Experimental

### 2.1. Synthesis

Platinum doped porous ceria, and palladium doped porous ceria were prepared using Palladium(II) chloride ($PdCl_2$, Aldrich) and Chloroplatinic acid hexahydrate ($H_2PtCl_6 \cdot 6H_2O$, Aldrich) without any treatment or purification as sources of noble metals. Additionally, they were prepared in different ratios (0.5, 1, 2.5, and 5 wt%) to study the catalytic activity of noble metals doped porous ceria.

During a typical synthesis, the dissolution of 5 g of cerium nitrate hexahydrate took place in 5 g of deionized water. Subsequently, 1 g of citric acid was introduced, and the appropriate stoichiometric quantity of metal salt was added to the crucibles. The resulting mixture was agitated until complete dissolution took place. The ensuing solution was then transferred to a porcelain crucible and subjected to a drying process at a temperature of 363 K (the optimum temperature for forming a foam-like structure from the formed gel) for a duration of 24 h. Ultimately, the resulting solid material underwent calcination in a muffle furnace in air under static conditions at 823 K for a period of 180 min. This process was conducted using a heating ramp characterized by a rate of 18 K per minute.

### 2.2. Characterization

Various techniques were employed for the characterization of the synthesized materials. X-ray diffractometer (XRD) analysis was conducted using a Shimadzu LabX-6000 diffractometer with CuK radiation ($\lambda = 1.54056$), operating at 40 kV and 30 mA, with a scanning range between 20–70° $2\theta$. ICP elemental analysis (Thermo Scientific, ICAP 7000 series) was used to calculate

Open Access Article. Published on 02 April 2024. Downloaded on 2/12/2026 6:44:27 AM.
This article is licensed under a Creative Commons Attribution-NonCommercial 3.0 Unported Licence.

each sample's exact amount of noble metals. Elemental composition, morphology, and energy mapping were obtained through a JEOL JSM 6310 scanning electron microscope (SEM) coupled with an EDX system, operating at 20 kV. Nitrogen adsorption/desorption isotherms at 77 K were recorded using a Quanta Chrome NOVA2000e. Pore size distribution was determined by the adsorption branch and the Barret–Joyner–Halenda (BJH) model. The surface area ($S_{BET}$) was calculated using the BET method, and mesopore volume ($V_{meso}$) was determined using the *t*-plot method (XPS) analysis was conducted utilizing an ESCALAB 250Xi instrument with a monochromatic Al Kα X-ray source (1486.6 eV). A 6 mm aperture was employed for the input lens. All spectra were acquired using monochromatized aluminum radiation. The X-ray source had a 12 kV acceleration voltage and a power output of 120 W. A survey spectrum was acquired spanning the binding energy range of 0 to 1200 eV, with a 10 eV pass energy and a 0.1 eV step size. The acquired spectra were evaluated using Origin Pro-8.5 software. This comprehensive XPS setup and analysis allow for detailed investigations into the elemental composition and chemical states of the analyzed samples. High-resolution transmission electron microscopy (HR-TEM) analysis was conducted using a Philips CM30UT electron microscope equipped with a field emission gun operating at 300 kV. For sample preparation, a copper-supported carbon polymer grid was utilized. A few droplets of a ground sample suspension in ethanol were placed on the grid, followed by drying at room temperature. This enabled the mounting of the samples for subsequent analysis.

### 2.3. The activity performance study

The hydrogenation of cyclohexene was executed in a semi-batch Parr reactor, as illustrated in Fig. 1. This reactor was equipped with a mixer capable of variable stirring speeds up to 800 rpm, featuring a maximum temperature of 453 K and a maximum pressure of 21 atm. The apparatus was further enhanced with an automated temperature control and pressure recording system. The liquid temperature within the reactor could be precisely controlled within a range of ±1 K. A high-precision pressure transducer with an accuracy of ±1 kPa was employed to measure pressure. The experimental procedure involved introducing 25 ml of cyclohexene and 0.25 g of catalyst into the reactor. The hydrogenation process was carried out under the specified conditions of 750 rpm stirring speed, 3 atm pressure at 393 K, and the duration of one hour. Following the reaction, the generated gas was released, and the reactor was gradually cooled down to room temperature. The resulting solution was then filtered, and the final product was analysed using gas chromatography (GC). Gas chromatography (GC) analysis was conducted utilizing a SHIMADZU GC-2014 instrument. The configuration featured an RTX-5(G27) packed column with dimensions of 4 m × 0.32 mm × 0.5 μm film thickness, along with a flame ionization detector (FID). Nitrogen ($N_2$) gas was employed as the carrier gas, while hydrogen ($H_2$) and air served as the FID gases. The conversion of cyclohexene (CXE) was calculated as following.

Top of the form

$$\text{Conversion} = \frac{[\text{CXE}]_0 - [\text{CXE}]_t}{[\text{CXE}]_0} \times 100$$

where $[\text{CXE}]_0$ is the concentration of cyclohexene at zero time, $[\text{CXE}]_t$ is the concentration of cyclohexene at ($t$) time. Moreover, the turnover frequency (TOF) was calculated as following

$$\text{TOF} = \frac{[\text{CXE}]_0 - [\text{CXE}]_t}{[\text{Pt or Pd}] \times \text{time (s)}}$$

where [Pt or Pd] is the concentration of Pt or Pd, while the time of reaction was calculated in seconds.

## 3. Results

### 3.1. Characterization data

The XRD analysis of the Pd–$CeO_2$ and Pt–$CeO_2$ catalysts, as illustrated in Fig. 2, reveals prominent diffraction peaks at 2$\theta$ values of 28.58°, 33.18°, 47.61°, and 56.49°, corresponding to

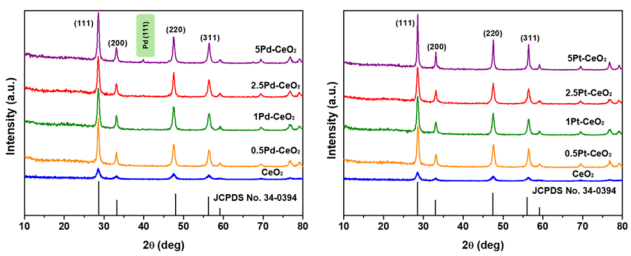


Fig. 2 XRD patterns of the prepared (a) Pd–$CeO_2$, and (b) Pt–$CeO_2$ samples.

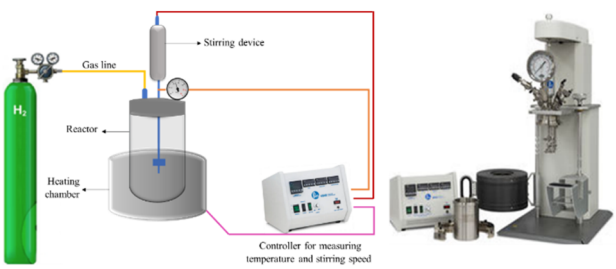


Fig. 1 Schematic diagram the Parr reactor components and reactor picture.

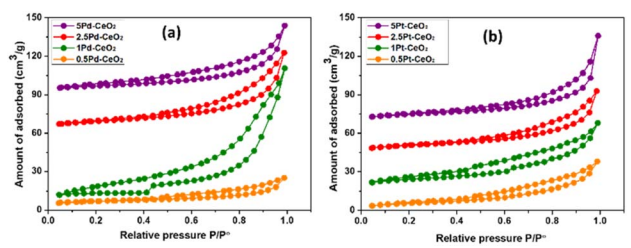


Fig. 3 The $N_2$ sorption isotherms of the prepared (a) Pd–$CeO_2$ and (b) Pt–$CeO_2$.


© 2024 The Author(s). Published by the Royal Society of Chemistry

Open Access Article. Published on 02 April 2024. Downloaded on 2/12/2026 6:44:27 AM. This article is licensed under a Creative Commons Attribution-NonCommercial 3.0 Unported Licence.

Table 1 The textural properties of porous ceria and (Pd and Pt) doped porous ceria nanoparticles

| Sample | Pd or Pt content (wt%)[a] | Surface area ($m^2$ $g^{-1}$)[b] | Pore volume ($cm^3$ $g^{-1}$)[b] | Pore size (nm)[b] |
|---|---|---|---|---|
| Porous $CeO_2$ | 0 | 47.18 | 0.138 | 2.8 |
| 0.5Pd–$CeO_2$ | 0.493 | 51.11 | 0.031 | 2.88 |
| 1Pd–$CeO_2$ | 0.996 | 46.45 | 0.091 | 2.71 |
| 2.5Pd–$CeO_2$ | 2.502 | 25.64 | 0.133 | 2.66 |
| 5Pd–$CeO_2$ | 4.997 | 15.45 | 0.079 | 1.99 |
| 0.5Pt–$CeO_2$ | 0.496 | 40.24 | 0.057 | 2.74 |
| 1Pt–$CeO_2$ | 1.006 | 25.55 | 0.078 | 2.79 |
| 2.5Pt–$CeO_2$ | 2.435 | 22.37 | 0.072 | 2.75 |
| 5Pt–$CeO_2$ | 4.994 | 19.9 | 0.101 | 2.56 |

[a] As obtained from ICP elemental analysis. [b] As obtained from Nitrogen sorption measurements.

the (111), (200), (220), and (311) crystal planes of the cubic fluorite structure of $CeO_2$, respectively (JCPDS 34-0394). However, there is an absence of observable diffraction peaks associated with metallic Pd in the samples with Pd loading less than 5 wt%, possibly due to the very small crystal size of metallic Pd or the formation of single-atom Pd, both are too small to be detected by this analysis technique. Same result was obtained in the case of Pt–$CeO_2$ sample. However, in 5Pd–$CeO_2$ sample, a peak emerges at $2\theta$ 39.95°, which corresponding to metal Pd (111) was observed.[27,28]

The $N_2$ adsorption/desorption isotherms of the synthesized catalysts (Pd–$CeO_2$ and Pt–$CeO_2$) are depicted in Fig. 3. All samples exhibit the characteristic shape of an IV-type isotherm with a H3 hysteresis loop at various $P/P^o$ values, signifying the presence of mesoporous structures in the prepared catalysts. The formation of the hysteresis loop can be attributed to the capillary condensation of $N_2$ molecules within the pore structures of the Pd–$CeO_2$ and Pt–$CeO_2$ catalysts.[29]

The surface areas, pore volume and pore size are listed in Table 1. The Brunauer–Emmett–Teller (BET) area of the Pd–$CeO_2$ (0.5%) sample is estimated to be 51 $m^2$ $g^{-1}$ and decreases to 15.45 $m^2$ $g^{-1}$ for Pd–$CeO_2$ (5%) after increase loading of Pt, additionally, the same behaviour presented for the Pt–$CeO_2$ which the surface area decreased from 40.24 $m^2$ $g^{-1}$ to 19.9 $m^2$ $g^{-1}$ with increase content of Pt up to 5%.[30] This can be explained by the formation of Pt or Pd nanoparticles which cause partial blocking in the channels of the porous ceria, and hence, the overall BET surface area deceased.

Scanning electron microscopy (SEM) was used to visualize the structure of the prepared materials Pd–$CeO_2$ and Pt–$CeO_2$ and the obtained micrographs are presented in Fig. 4 and 5. Micrographs reveal the formation of porous foam-like network of agglomerated interconnected particles with a three-dimensional porous structure in the entire prepared samples. Moreover, the wall thickness seems to be increased with noble metals content (0.5 to 5%). More importantly, there is no evidence for the formation of any bulky crystals of metallic Pd or Pt, or the oxide form of both. The obtained result agrees the obtained XRD result.

Fig. 6 presents the EDX spectra for the 5Pd–$CeO_2$ and 5Pt–$CeO_2$ samples. The spectra indicate the presence of Ce, O, and either Pd or Pt in the samples. No other elements are detected, except for carbon, which can be attributed to the carbon tape used during the analysis. This outcome provides a strong

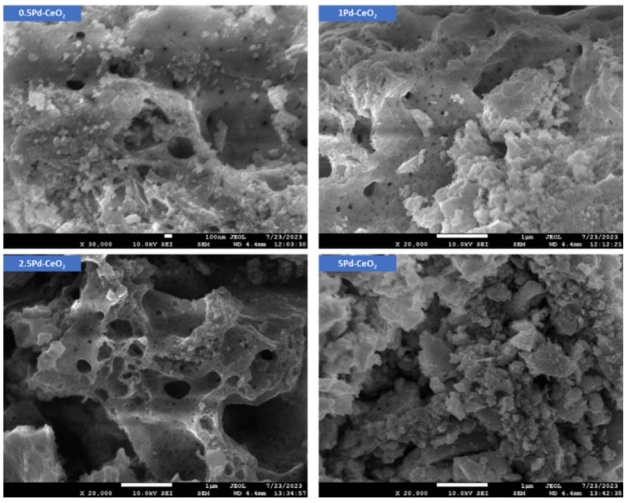


Fig. 4 The SEM micrographs of the prepared Pd-doped porous ceria samples.

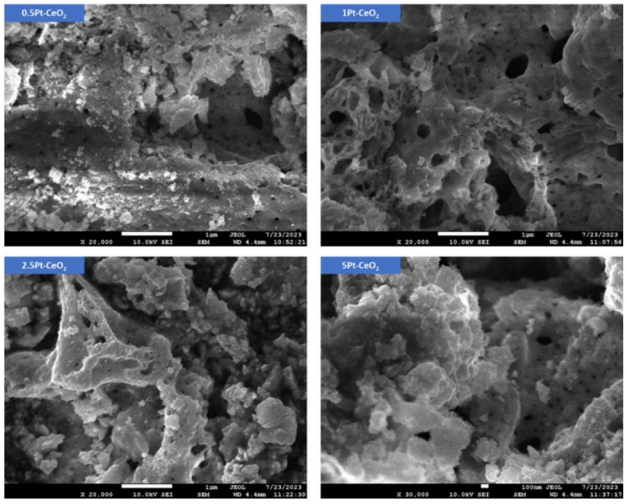


Fig. 5 The SEM micrographs of the prepared Pt-doped porous ceria samples.

© 2024 The Author(s). Published by the Royal Society of Chemistry

Open Access Article. Published on 02 April 2024. Downloaded on 2/12/2026 6:44:27 AM.
This article is licensed under a Creative Commons Attribution-NonCommercial 3.0 Unported Licence.

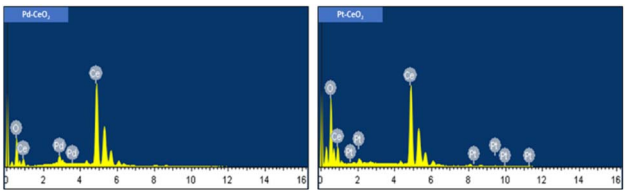


Fig. 6 EDX analysis of Pd doped porous ceria and Pt-doped porous ceria samples.

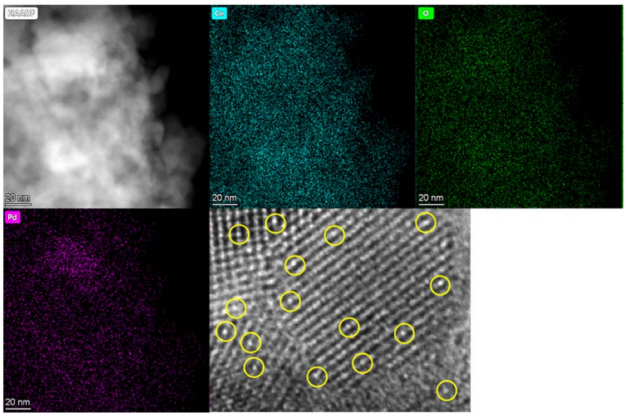


Fig. 7 High-angle annular dark-field scanning transmission electron microscopy (HAADF–STEM) micrographs and corresponding Cs-corrected micrograph of 5Pd–$CeO_2$ sample.

indication of the purity of the prepared samples, as no extraneous elements are observed.

The HAADF–STEM technique was applied to investigate the distribution of Pt and Pd in the ceria framework. The obtained elemental mapping of 5Pt–$CeO_2$ and 5Pd–$CeO_2$ are presented in Fig. 7 and 8; respectively. The obtained micrographs show the spatial distribution of ceria, oxygen Pd and Pt and they indicate that Pt and Pd uniformly distributed throughout the entire porous ceria sample. It must also be emphasized that no additional elements were detected. More importantly, in Fig. 9, the single atoms of Pt and Pd are clearly presented as a bright

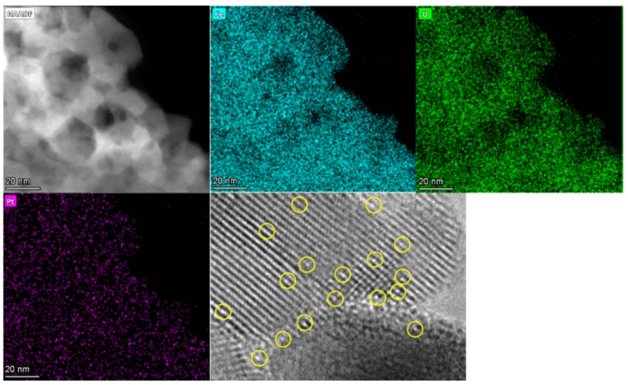


Fig. 8 High-angle annular dark-field scanning transmission electron microscopy (HAADF–STEM) micrographs and corresponding Cs-corrected micrograph of 5Pt–$CeO_2$ sample.

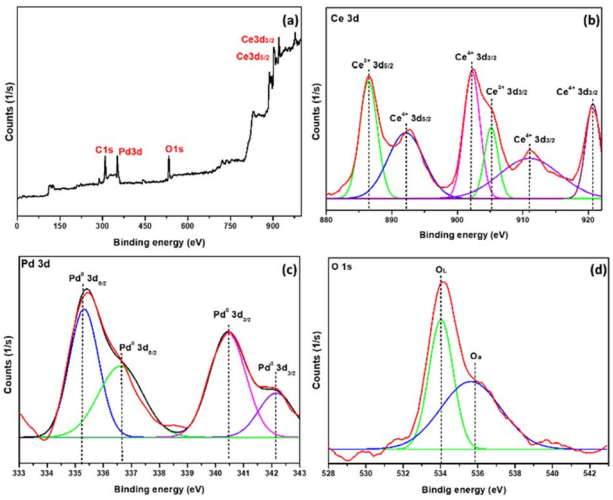


Fig. 9 XPS spectra of (a) survey scan XPS spectrum, (b) Ce3d (c) Pd3d of Pd–$CeO_2$ and (d) O1s.

dot as compared to the neighbouring Ce atoms due to their larger atomic number.[31]

XPS was applied to assess the valence state of Pd, Pt, Ce, and O in order to determine the nature of the active sites in Pd–$CeO_2$ and Pt–$CeO_2$. The obtained spectra and their deconvolution are presented in Fig. 9 and 10 for 5Pd–$CeO_2$ and 5Pt–$CeO_2$, respectively.

Panel (a) of Fig. 9 and 10, shows the survey spectrum of the whole prepared samples, while panel (b) shows the Ce3d spectra and their deconvolution into six components. These components correspond to the spin–orbit splitting of $Ce3d_{5/2}$ and $Ce3d_{3/2}$, indicating that $CeO_2$ contains both $Ce^{3+}$ and $Ce^{4+}$ oxidation states due to the spin doublet's separation. Peaks belonging to $Ce3d_{5/2}$ ionization exist at binding energies 886.4 and 892.1 eV, whereas those corresponding to $Ce3d_{3/2}$ ionization appear at 901.9, 905.3, 910.9, and 920.6 eV. The peaks at 886.4 and 905.3 eV correspond to $Ce^{3+}$3d states, whereas the peaks at 892.1, 901.9, 910.9, and 920.6 eV correspond to $Ce^{4+}$3d

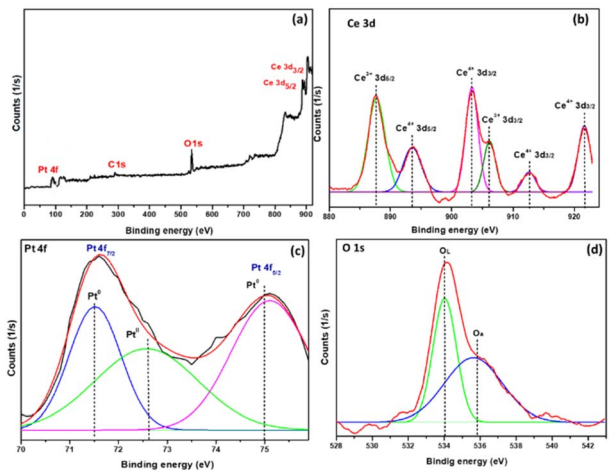


Fig. 10 XPS spectra of (a) survey scan XPS spectrum, (b) Ce3d (c) Pt4f, and (d) O1s.


© 2024 The Author(s). Published by the Royal Society of Chemistry

Open Access Article. Published on 02 April 2024. Downloaded on 2/12/2026 6:44:27 AM.
This article is licensed under a Creative Commons Attribution-NonCommercial 3.0 Unported Licence.

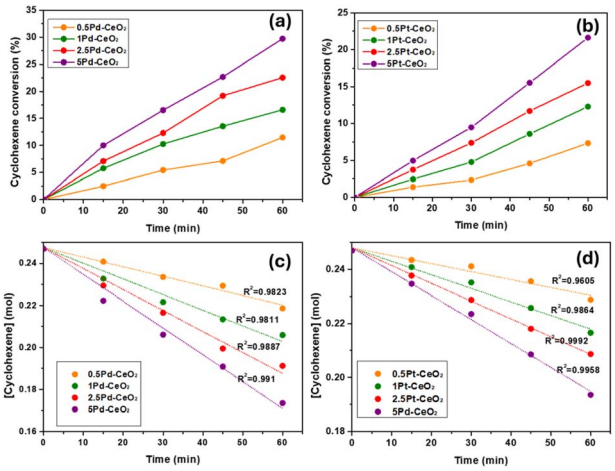


Fig. 11 Top panels: the formation of cyclohexane (%) over: (a) Pd–$CeO_2$ samples and (b) Pt–$CeO_2$ samples. Bottom panels: the fitting of zero order kinetic model for (c) Pd–$CeO_2$ samples and (d) Pt–$CeO_2$.

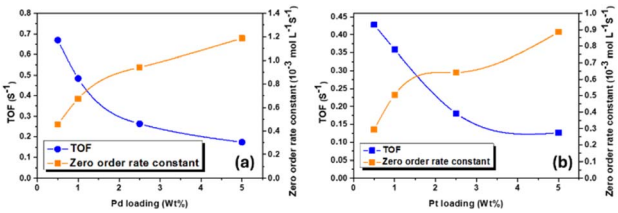


Fig. 12 The turnover frequency TOF ($s^{-1}$) and the zero order rate constant (mol $L^{-1}$ $s^{-1}$) as a function of (a) Pd and (b) Pt loading (wt%).

states. This denotes Ce's fundamental valence state as +4.[32] According to reports, $CeO_2$ is not reducible by $H_2$ at 200 °C.[33] However, the introduction of metallic Pd species has been shown to facilitate the transfer of hydrogen from metallic Pd to the $CeO_2$ surface. Consequently, this transfer promotes the reduction of oxygen species on the $CeO_2$ surface, leading to the formation of oxygen vacancies.[34]

In Fig. 9(c), the Pd3d XPS spectrum is illustrated. Notably, the two prominent peaks observed at 335.2 and 340.5 eV correspond to the characteristic XPS peaks of $Pd^0$, originating from the $Pd3d_{3/2}$ and $Pd3d_{5/2}$ orbitals, respectively. Weak XPS peaks corresponding to $Pd^{2+}$ species are also discernible at binding energies of 336.7 and 342.2 eV. This suggests that metallic Pd species predominantly exist on the surface of Pd–$CeO_2$ catalysts in a zero-valent state. The presence of trace $Pd^{2+}$ species may be attributed to electronic interactions between metallic Pd and $CeO_2$ supports, indicating electron transfer from metallic Pd to the $CeO_2$ support. Moreover, based on morphology studies, Pd–$CeO_2$ exhibits mesoporous structures, facilitating the high dispersion of metallic Pd on their surface and enhancing their interaction.[35] Furthermore, in Fig. 10(c), the XPS spectrum of the Pt–$CeO_2$ catalysts shows typical peaks of Pt $4f_{7/2}$ and $4f_{5/2}$. Both peaks were deconvoluted into three sub-peaks representing oxidized and metallic Pt. The two deconvoluted sub-peaks at 71.5 and 75.1 eV are assigned to $Pt^0$, whereas the other peak at 72.6 eV corresponds to the $Pt^{2+}$ specie, as previously described in ref. 36 and 37. Finally, the XPS spectrum of O1s is shown in panel (d) of Fig. 9 and 10. The O1s XPS spectra can be divided into two independent XPS peaks. The XPS peak from 532 to 334.5 eV is the characteristic of lattice oxygen, the peak at 535 to 536.5 eV belongs to the adsorbed oxygen $O^-$ on the Pd–$CeO_2$ and Pt–$CeO_2$ surface.

### 3.2. The catalytic performance

Several blank experiments were performed in the beginning of the study to confirm the catalytic process and to determine the best operating conditions. Cyclohexene was hydrogenated without any catalyst up to 393 K and 10 atm of pure $H_2$ gas, however no cyclohexane could be observed. Same result was obtained when bare $CeO_2$ was applied to catalyse the hydrogenation reaction. In another experiment, commercial Pt nanoparticles successfully activated 5.6% conversion of cyclohexene to cyclohexane. In a third experiment, Pd–$CeO_2$ and Pt–$CeO_2$ samples were not able to activate the conversion of cyclohexene at ambient conditions, room temperature and 1 atm of $H_2$ gas.

Table 2 The catalytic activity results of the investigated samples in the hydrogenation of cyclohexene to cyclohexane

| Sample | $P$ (atm) | $T$ (K) | Con[a] (%) | Sel[b] (%) | TOF[c] ($s^{-1}$) | $(R^2)^d$ | $(k)^e$ |
|---|---|---|---|---|---|---|---|
| No catalyst | 3 | 393 | >1 | 100 | — | — | — |
| $CeO_2$ | 3 | 393 | >1 | 100 | — | — | — |
| Pt NPs[f] | 3 | 393 | 5.6 | 100 | 0.0015 | — | — |
| 5Pd–$CeO_2$ or 5Pt–$CeO_2$ | 1 | 298 | >1 | 100 | — | — | — |
| 0.5Pd–$CeO_2$ | 3 | 393 | 11.5 | 100 | 0.669 | 0.982 | 0.454 |
| 1Pd–$CeO_2$ | 3 | 393 | 16.6 | 100 | 0.484 | 0.981 | 0.675 |
| 2.5Pd–$CeO_2$ | 3 | 393 | 22.5 | 100 | 0.263 | 0.989 | 0.942 |
| 5Pd–$CeO_2$ | 3 | 393 | 29.7 | 100 | 0.176 | 0.991 | 1.188 |
| 0.5Pt–$CeO_2$ | 3 | 393 | 7.33 | 100 | 0.428 | 0.961 | 0.294 |
| 01Pt–$CeO_2$ | 3 | 393 | 12.3 | 100 | 0.359 | 0.986 | 0.505 |
| 2.5Pt–$CeO_2$ | 3 | 393 | 15.5 | 100 | 0.181 | 0.999 | 0.641 |
| 5Pt–$CeO_2$ | 3 | 393 | 21.6 | 100 | 0.126 | 0.996 | 0.886 |
| Pd-*c*-$CeO_2$[g] | 3 | 393 | 18.6 | 100 | 0.107 | 0.992 | 0.314 |

[a] Conversion of cyclohexene. [b] Selectivity of cyclohexane. [c] Turnover frequency. [d] Correlation coefficient. [e] Zero order rate constant ($10^{-3}$ mol $L^{-1}$ $s^{-1}$). [f] Commercial Pt nanoparticles. [g] 5 wt% of Pd doped commercial ceria.

© 2024 The Author(s). Published by the Royal Society of Chemistry

Open Access Article. Published on 02 April 2024. Downloaded on 2/12/2026 6:44:27 AM.
This article is licensed under a Creative Commons Attribution-NonCommercial 3.0 Unported Licence.

Based on optimization study, the activity of the prepared samples could be observed at 393 K and 3 atm of $H_2$ pressure.

The production of cyclohexane over Pd–$CeO_2$ and Pt–$CeO_2$ samples is presented in Fig. 11 panels (a) and (b), respectively. The conversion% was found to be increased with the noble-metal loading. In general, Pd–$CeO_2$ was found to be more active than Pt–$CeO_2$ sample although the entire samples in the series were able to activate the reaction. The best conversion was achieved over 5Pd–$CeO_2$ sample, in which 29.7% of cyclohexene was converted to cyclohexane after 60 min′s reaction. To investigate the kinetic of hydrogenation proves over the prepared samples, zero order model was applied. The concentration of cyclohexene (mole) was plotted as a function of reaction time and the calculated slope represented the rate constant of the reaction kinetic. The obtained data fitted perfectly with the suggested model with high calculated correlation coefficient ($R^2$) as shown in Fig. 11(c) and (d).

The calculated turnover frequency TOF ($s^{-1}$) and the zero order rate constant (mol $L^{-1}$ $s^{-1}$) were plotted as a function of Pd and Pt loading in Fig. 12(a) and (b), respectively. The rate constant of the investigated samples exhibited similar behaviour either for Pd–$CeO_2$ or Pt–$CeO_2$. The zero-order rate constant was found to be increased with the loading of Nobel metal concentration. However, TOF was found to be decreased with the Nobel metal loading, which is most likely due to the formation of nanoparticles and hence considerable amount of active phase are out of the catalytic process. The obtained results of the catalytic reaction as well as the blank reactions are summarized in Table 2.

Furthermore, one additional sample was prepared for comparison purpose, 5 wt% Pd doped commercial ceria sample. The activity of the sample was small compared to 5Pd–$CeO_2$ sample. This can be explained by the unique porous system of the prepared sample, in addition to the higher surface area than commercial ceria sample, and the oxygen vacancies rich surface of the porous ceria sample.[38] Finally, the most performed catalysts, 5Pd–$CeO_2$ and 5Pt–$CeO_2$ were subjected to reusability study after collecting the applied catalysts by hot-filtration technique. Each sample was used to catalyse five consecutive reactions without treatment but drying over night at 333 K. The obtained cyclohexene conversion% is plotted in Fig. 13. The investigated catalysts were able to catalyse the five runs and the obtained conversion% was comparable. The small loos in activity can be related either to the leaching of Pt or Pd from $CeO_2$ framework (ICP elemental analysis showed that almost 2.5–3.8% of noble metals was lost after the 5th run), or due to the accumulation of the organic species on the catalytic active sites.

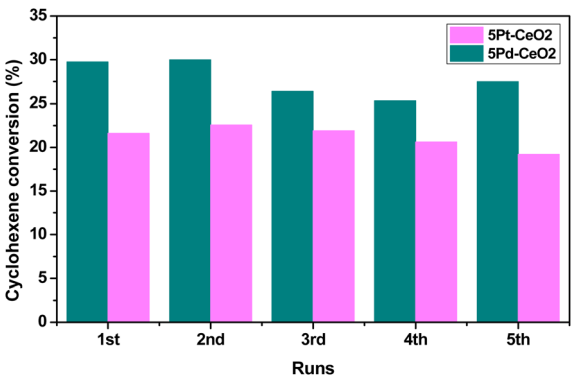


Fig. 13 The cyclohexene conversion (%) over the same sample of 5Pd–$CeO_2$ and 5Pt–$CeO_2$ for consecutive five runs without any treatment.

# 4. Discussion

## 4.1. The formation of single-atom Pd or Pt

Noble metals like platinum (Pt) and palladium (Pd) are known for their catalytic properties, especially when supported on cerium dioxide ($CeO_2$) nanoparticles. The formation of single-atom noble metal catalysts on $CeO_2$ has gained interest due to their high catalytic activity and selectivity in various reactions. The formation of single atoms of noble metals on the surface of $CeO_2$ is influenced by several properties of $CeO_2$, which leads to creating the stabilization of dispersed metal atoms. Such as presence of oxygen vacancies that provides coordination sites for the noble metal atoms, allowing them to bind strongly and disperse as isolated atoms on the surface of ceria.[39] Redox properties which is the transformation between $Ce^{3+}$ and $Ce^{4+}$ in $CeO_2$, the robust electronic interaction facilitates a strong binding of surface oxygen to metal atoms. In this scenario, metal atoms exhibit a preference for bonding with oxygen rather than forming metal–metal bonds. Consequently, the favourable condition for single atomic dispersion is often observed on $CeO_2$, rather than the aggregation into nanoparticles.[40] Strong Metal-Support Interaction (SMSI): $CeO_2$ is known to exhibit SMSI with certain noble metals. This strong interaction involves the exchange of electrons between the metal and the support, leading to enhanced stability and dispersion of single metal atoms. The combination of these properties creates a favourable environment for the formation of single metal atoms on the $CeO_2$ surface, providing unique catalytic properties that are advantageous in various applications.

## 4.2. The proposed mechanism

The hydrogenation mechanism of cyclohexene by using molecular hydrogen over Pt, or Pd–$CeO_2$ can be explained as following steps:

1 Adsorption step: $H_2$ molecules are adsorbed and activated through weaken the H–H bond and facilitate the formation of reactive hydrogen species, over noble metal single-atoms and/or the formed nanoparticles. On the other hand, $CeO_2$ support is strongly participate in the adsorption of cyclohexene double bonds due to the presence of oxygen vacancies (Vo) in the ceria lattice.

2 Reaction step: the activated hydrogen interacts with the double bond in cyclohexene, leading to the addition of hydrogen atoms and the reduction of the double bond to form cyclohexane.

3 Desorption step: the formed cyclohexane molecules migrate away from the surface of the catalyst, while Pd or Pt


© 2024 The Author(s). Published by the Royal Society of Chemistry

Open Access Article. Published on 02 April 2024. Downloaded on 2/12/2026 6:44:27 AM.
This article is licensed under a Creative Commons Attribution-NonCommercial 3.0 Unported Licence.

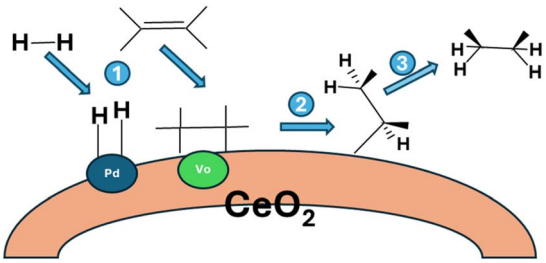


Fig. 14 The proposed mechanism for the hydrogenation of single atom Pd or Pt incorporated oxygen-vacancies rich mesoporous ceria.

Table 3 The activity comparison between Pd and Pt incorporated porous ceria and other reported catalysts in the liquid phase hydrogenation of cyclohexene

| Support | Noble metal | Loading (%) | Temp (K) | Pressure (atm) | TOF ($s^{-1}$) | Ref. |
|---|---|---|---|---|---|---|
| Porous $CeO_2$ | Pd | 0.5 | 393 | 3 | 0.669 | Current |
| Porous $CeO_2$ | Pt | 0.5 | 393 | 3 | 0.428 | Current |
| Zeolite Y | Pt | 0.57 | 298 | 5 | 0.231 | 9 |
| Mordenite | Pt | 0.59 | 298 | 5 | 0.31 | 9 |
| TUD-1 | Pt | 0.5 | 298 | 5 | 1.08 | 41 |
| $Al_2O_3$ | Pt | 1 | 393 | 1 | 0.9 | 42 |
| $SiO_2$ | Rh | 0.1 | 343 | 4 | 0.13 | 43 |

active sites undergo regeneration to be ready for a new reaction. This reusability makes palladium a cost-effective and sustainable catalyst for industrial processes.

In Fig. 14, a simple diagram is proposed to explain the hydrogenation of cyclohexene over single-atom Pd or Pt incorporated oxygen-vacancies rich porous ceria nanoparticles.

### 4.3. Comparison with other supported catalysts

The comparison with other reported catalysts is a challenging because the scarcity of research around the liquid-phase cyclohexene hydrogenation. In Table 3, the hydrogenation of liquid phase hydrogenation over different supported catalysts. The comparison showed that porous ceria is a competitor support for the noble metal active phase in the hydrogenation reaction. Pt and Pd incorporated porous ceria showed better activity than noble metals supported zeolite Y,[9] mordenite,[9] and mesoporous silica.[41] Ceria can adsorb cyclohexene due to its unique surface properties and interactions with the molecule. The oxygen vacancies on the ceria surface provide active sites for adsorption, allowing unsaturated carbon atoms in cyclohexene to interact with surface oxygen atoms. Additionally, ceria's Lewis acid–base interactions, high surface area, and redox properties contribute to the strong binding and adsorption of cyclohexene. These characteristics enable ceria to effectively adsorb cyclohexene molecules, making it a suitable catalyst for related chemical reactions. However, Pt incorporated mesoporous silica (TUD-1)[42] and alumina[43] exhibited better activity. The effectiveness of tiny noble metals on $CeO_2$ as catalysts can be influenced by various factors, including the interaction between metals and the support, the structure of $CeO_2$, and the condition of noble metals. Initially, broadly speaking, the interplay between metal and support can enhance the catalytic efficiency of catalysts. Firstly, the robust connection between metals and supports can anchor noble metals at specific locations, preventing aggregation and the loss of activation. Secondly, this interaction can boost interfacial electron transfer and molecular adsorption modulation, thereby influencing the catalyst's activity, selectivity, and stability.

This comparison shows that oxygen-vacancies rich porous ceria is an interesting support, and it opens the door for more development to increase the surface area of porous ceria and hence improve its performance.

## 5 Conclusions

Pd or Pt with different content was successfully incorporated into porous ceria by using one-step synthesis procedure based on flash-combustion technique. The characterization confirmed the formation of well-distributed single-atom Pt or Pd throughout the entire surface of the oxygen-vacancies rich ceria support. Few nanoparticles of Pd were also observed in the high loading of Pd–$CeO_2$ sample. The hydrogenation of cyclohexene was performed under solvent-free condition and activated by the prepared catalysts and the obtained results were comparable with other reported catalysts. Moreover, the catalysts exhibited good activity up to five continuous runs. The kinetics of the hydrogenation reaction was investigated, and the obtained results were perfectly fit with zero-order kinetic model.

## Author contributions

The two authors have equal contribution in conceptualization, methodology, formal analysis, investigation, and writing original draft preparation. M. S. H took the lead of supervision, project administration, and funding acquisition. The two authors have read and agreed to publish the current version of the manuscript.

## Conflicts of interest

There are no conflicts to declare.

## Acknowledgements

The authors are greatly thankful to the Deanship of Scientific Research at King Khalid University, Saudi Arabia for funding the current research in the framework of Large Group Research Projects under Grant no. RGP2/106/45.

## Notes and references

1 J. N. Reek, B. de Bruin, S. Pullen, T. J. Mooibroek, A. M. Kluwer and X. Caumes, *Chem. Rev.*, 2022, **122**(14), 12308–12369.
2 X. Zhao, Y. Chang, W. J. Chen, Q. Wu, X. Pan, K. Chen and B. Weng, *ACS Omega*, 2021, **7**(1), 17–31.

Open Access Article. Published on 02 April 2024. Downloaded on 2/12/2026 6:44:27 AM. This article is licensed under a Creative Commons Attribution-NonCommercial 3.0 Unported Licence.

3 P. Lozano-Reis, H. Prats, P. Gamallo, F. Illas and R. Sayos, *ACS Catal.*, 2020, **10**(15), 8077–8089.
4 S. R. Schmidt, *The Raney® catalyst legacy in hydrogenation, from Hydrogenation Catalysts and Processes*, Walter de Gruyter GmbH, Berlin, 2018, pp. 19–42.
5 Z. Lin, B. Huang, L. Ouyang and L. Zheng, *Molecules*, 2022, **27**(11), 3576.
6 Z. Liu, S. Liu, Z. Li, Z. Liu and S. Liu, *Catalytic Technology for Selective Hydrogenation of Benzene to Cyclohexene*, Springer, Singapore, 2020, pp. 1–32.
7 J. A. Poveda-Giraldo, J. C. Solarte-Toro and C. A. Alzate, *Renewable Sustainable Energy Rev.*, 2021, **138**, 110688.
8 L. H. Gong, Y. Y. Cai, X. H. Li, Y. N. Zhang, J. Su and J. S. Chen, *Green Chem.*, 2014, **16**(8), 3746–3751.
9 M. S. Hamdy, F. A. Alqahtani, M. Shkir, K. F. Fawy, M. Benaissa, M. B. B. Hamida and N. Elboughdiri, *Catalysts*, 2022, **12**(10), 1106.
10 Y. Gu, J. R. Norton, F. Salahi, V. G. Lisnyak, Z. Zhou and S. A. Snyder, *J. Am. Chem. Soc.*, 2021, **143**(25), 9657–9663.
11 S. Peil, G. Bistoni, R. Goddard and A. Fürstner, *J. Am. Chem. Soc.*, 2020, **142**(43), 18541–18553.
12 K. Cunningham, M. Enmeier, G. Huldin, G. Bacchin, K. Grossman, G. Recker and B. Mattson, *J. Chem. Educ.*, 2023, **100**(5), 2080–2085.
13 N. M. Martin, P. Velin, M. Skoglundh, M. Bauer and P. A. Carlsson, *Catal. Sci. Technol.*, 2017, **7**(5), 1086–1094.
14 Q. Sun, N. Wang and J. Yu, *Adv. Mater.*, 2021, **33**(51), 2104442.
15 X. Chen, X. B. Wang, S. Han, D. Wang, C. Li, W. Guan and C. iang, *ACS Appl. Mater. Interfaces*, 2021, **14**(1), 590–602.
16 D. Eberhardt, P. Migowski, S. R. Teixeira and A. F. Feil, *J. Nanosci. Nanotechnol.*, 2018, **18**(3), 2075–2078.
17 A. Patel and N. Narkhede, *Eur. J. Inorg. Chem.*, 2019, **3**, 423–429.
18 M. Benaissa, A. M. Alhanash, M. Eissa, A. Aldalbahi, S. Alzahly, M. Rahaman and M. S. Hamdy, *J. Porous Mater.*, 2020, **27**, 1735–1743.
19 M. Benaissa, A. M. Alhanash, A. T. Mubarak, M. Eissa, T. Sahlabji and M. S. Hamdy, *RSC Adv.*, 2018, **8**(60), 34370–34373.
20 L. Chen, P. Verma, K. Hou, Z. Qi, S. Zhang, Y.-S. Liu and J. Guo, *Nat. Commun.*, 2022, **13**, 1092.
21 N. Zhang, C. Ye, H. Yan, L. Li, H. He, D. Wang and Y. Li, *Nano Res.*, 2020, **13**, 3165–3182.
22 Y. Wang, G. Song, Z. Xu, F. Rosei, D. Ma and G. Chen, *J. Mater. Chem. A*, 2016, **4**(37), 14148–14154.
23 G. Spezzati, Y. Su, J. P. Hofmann, A. D. Benavidez, A. T. DeLaRiva, J. McCabe and E. J. Hensen, *ACS Catal.*, 2017, **7**(10), 6887–6891.
24 K. Yuan, Y. Guo, Q. Lin, L. Huang, J. T. Ren, H. C. Liu and Y. W. Zhang, *J. Catal.*, 2021, **394**, 121–130.
25 K. Khivantsev, C. G. Vargas, J. Tian, L. Kovarik, N. R. Jaegers, J. Szanyi and Y. Wang, *Angew. Chem., Int. Ed.*, 2021, **60**(1), 391–398.
26 B. Wu, T. Lin, R. Yang, M. Huang, H. Zhang and Y. Sun, *Green Chem.*, 2021, **23**(13), 4753–4761.
27 T. Li, D. Xia, G. Zhou, H. Xie, Z. Jiao and X. Zhang, *Catal. Commun.*, 2018, **112**, 35–38.
28 X. Gao, Y. Bai, H. Zhang and X. Wang, *ACS Omega*, 2023, **8**(7), 6791–6800.
29 M. A. Aziz, A. A. Jalil, S. Triwahyono and M. W. A. Saad, *Chem. Eng. J.*, 2015, **260**, 757–764.
30 G. Zhou, T. Li, J. Chen, L. Deng and H. Xie, *Int. J. Hydrogen Energy*, 2021, **46**(27), 14540–14555.
31 C. Wang, S. Mao, Z. Wang, Y. Chen, W. Yuan and Z. Jiang, *Chem*, 2020, **6**(3), 752–765.
32 S. Zeng, Y. Wang, S. Ding, J. J. Sattler, E. Borodina, L. Zhang and H. Su, *J. Power Sources*, 2014, **256**, 301–311.
33 Y. Gao, E. Hu, G. Yin and Z. Huang, *Fuel*, 2021, **302**, 121142..
34 B. Dai, G. Zhou, S. Ge, H. Xie, Z. Jiao, G. Zhang and K. Xiong, *Can. J. Chem. Eng.*, 2017, **95**(4), 634–642.
35 H. Q. Lin and Y. W. Chen, *J. Taiwan Inst. Chem. Eng.*, 2016, **67**, 69–73.
36 P. P. Kostrobij and B. M. Markovych, *Philos. Mag. Lett.*, 2019, **99**(1), 12–20.
37 S. Zhang, Z. Xia, T. Ni, Z. Zhang, Y. Ma and Y. Qu, *J. Catal.*, 2018, **359**, 101–111.
38 A. A. Atran and M. S. Hamdy, *Catalysts*, 2023, **13**(3), 523.
39 Z. Zhang, J. Tian, Y. Lu, S. Yang, D. Jiang, W. Huang and Y. Wang, *Nat. Commun.*, 2023, **14**(1), 1–10.
40 P. Bera and M. S. Hegde, *RSC Adv.*, 2015, **5**(115), 94949–94979.
41 A. M. Alhanash, F. A. Alqahtani, A. Aldalbahi, M. Rahaman, M. Benaissa and M. S. Hamdy, *Inorg. Chem. Commun.*, 2021, **127**, 108545.
42 M. Farajzadeh, H. Alamgholiloo, F. Nasibipour, R. Banaei and S. Rostamnia, *Sci. Rep.*, 2020, **10**(1), 1–9.
43 M. A. Gelesky, S. S. Chiaro, F. A. Pavan and J. Dupont, *Dalton Trans.*, 2007, **47**, 5549–5553.


© 2024 The Author(s). Published by the Royal Society of Chemistry